

Comparison of Omega-K and Backprojection regarding Spatial Resolution for Squinted Spotlight SAR with Motion Errors

Aron Sommer
Institut für Informationsverarbeitung
Leibniz Universität Hannover
Hannover, Germany
sommer@tnt.uni-hannover.de

Minh Phuong Nguyen
Institut für Informationsverarbeitung
Leibniz Universität Hannover
Hannover, Germany
nguyenmp@tnt.uni-hannover.de

Jörn Ostermann
Institut für Informationsverarbeitung
Leibniz Universität Hannover
Hannover, Germany
ostermann@tnt.uni-hannover.de

Abstract—The image quality of an image processing technique in a real airborne spotlight Synthetic Aperture Radar scenario mainly depends on its capability of correcting motion error effects. Therefore we compare the frequency domain imaging technique rotated Omega-K with explicit range cell migration correction with the time domain algorithm global Backprojection in their imaging quality by taking motion errors and scene size as well as the squint and the depression angles into account. The numerical investigations show that for a squint angle of 20° and a depression angle of 25° up to a limit of 5 m motion error magnitude Omega-K yields good image quality in terms of Integrated Side Lobe Ratio for point targets with 200 m ground range distance to the spot center. For larger motion errors or larger scene sizes the Backprojection algorithm should be used to guarantee image quality with the disadvantage of higher computational costs.

I. INTRODUCTION

In a real airborne Synthetic Aperture Radar (SAR) scenario, environmental influences like motion errors lead to low spatial resolution of the SAR image. Especially small airplanes, like unmanned aerial vehicles (UAVs), are vulnerable to motion errors. Frequency domain algorithms require a straight flight path and a constant velocity, therefore motion compensation techniques have been developed to remove the effects of motion errors in raw data. Time domain algorithms permit arbitrary flight paths, so that no motion compensation is necessary. However, the global Backprojection algorithm, as the most common representative of this algorithm-family, has high computational cost of $O(N^3)$, whereas the computationally efficient frequency domain method Omega-K performs only $O(N^2 \log_2 N)$ operations. Here N is the number of slow-time samples for an image with $N \times N$ pixels.

The quality produced by an image processing technique mainly depends on its capability of correcting motion error effects. Because the first order motion compensation of the standard squinted Omega-K algorithm uses the center beam approximation, only the spot center is perfectly focused. With increasing ground range distance to the spot center the spatial resolution decreases rapidly, so that we do not involve this algorithm in our comparison. The rotated Omega-K algorithm with explicit range cell migration correction [5]

was developed to perform a second motion compensation [6] in the squinted case. It compensates the residual phase error remaining from its first motion compensation [4] depending on the distance to every range cell. Consequently, the whole scene is better focused.

Moreover the global Backprojection algorithm [12] enables processing images with arbitrary center position, image-size and image-resolution. No additional motion compensation is necessary and no restriction of the scene size has to be considered.

Vu et. al. [7] and Hunter et. al. [8] compared the Omega-K algorithm with the fast factorized Backprojection in image quality. However, the squinted case was not considered and no qualitative evaluations regarding motion errors have been published.

For this reason, we focus on the problem of finding the limits of motion error magnitude between rotated Omega-K with explicit range cell migration correction [6] and global Backprojection [12] with respect to acceptable SAR image quality in terms of Integrated Side Lobe Ratio (ISLR). We assume that the real flight path is accurately measured by an onboard GPS/IMU system and thus available.

We find the range of applicability of both algorithms by computing the ISLR as a function of ground range distance to the scene center, motion error magnitude, squint angle and depression angle for several perturbed flight paths. Additionally, in order to reduce computational time we develop a technique for shifting an image in frequency domain that allows processing smaller SAR images (e.g. $8k \times 8k$ pixel instead of $64k \times 8k$) by Omega-K and avoids creating an image of the whole scene.

In the following, Section II introduces the signal model; Section III and V give a short summary of both compared algorithms. The technique for shifting an image in frequency domain is introduced in Section IV. Numerical experiments are presented in Section VI. The results including an example of an X-band system are shown in Section VII, followed by conclusions in Section VIII.

II. SIGNAL MODEL

Let an airplane fly with constant velocity $v_0 \in \mathbb{R}_+$ along a straight line $\gamma : \mathcal{L} \rightarrow \mathbb{R}^3$ of length $L \in \mathbb{R}_+$. This flight path is parameterized by $\gamma(s) = (v_0 s - L/2, y_0, z_0)^\top$ for slow time $s \in \mathcal{L} := [0, L/v_0]$ and constant $y_0, z_0 \in \mathbb{R}_+$.

We model motion errors by a 3D colored noise function $\mathbf{n}_\sigma : \mathcal{L} \rightarrow \mathbb{R}^3$, i.e. we use additive Gaussian white noise with standard deviation $\sigma \in \mathbb{R}_+$ and a lowpass-filter with fixed cutoff frequency of 1.5 Hz in x, y and 1.5 Hz in z . For the lowpass-filtering we choose a Hann window function. Thus, the perturbed flight path $\tilde{\gamma}_\sigma$ is generated by

$$\tilde{\gamma}_\sigma(s) = \gamma(s) + \mathbf{n}_\sigma(s), \quad s \in \mathcal{L}.$$

Note that the parameter σ controls the magnitude of the noise \mathbf{n}_σ . Furthermore, let the ground be a plane in the xy -axes at $z = 0$. The scene consists of one point target at $\mathbf{p}_t = (x_t, y_t, 0)^\top \in \mathbb{R}^3$ and is represented by the reflectivity function $V(x, y) = \delta(x - x_t, y - y_t)$ with $x, y \in \mathbb{R}$. This brings us to the signal model given by Cheney [9] of the received signal

$$\tilde{d}(t, s) = \int_{\mathbb{R}} g_c(\tau, s) p(t - \frac{2\tau}{c}) d\tau, \quad (1)$$

which depends on fast time $t \in \mathcal{T}$ with sampling time interval \mathcal{T} and slow time $s \in \mathcal{L}$. Let the pulse p be a chirped pulse with shape $p(t) = \text{rect}(\frac{t}{T}) e^{-2\pi i f_c t} e^{i\pi \gamma t^2}$ for $t \in \mathbb{R}$, f_c the carrier frequency, γ the chirp rate, T the pulse duration and c the speed of light. Here the circular radon transform g_c of the reflectivity function V has the form

$$g_c(\tau, s) = \int_{\mathbb{R}^2} V(x, y) \delta(\tau - R(s, x, y)) dx dy = \delta(\tau - R(s, x_t, y_t)),$$

with distance $R(s, x, y) := \|\tilde{\gamma}_\sigma(s) - (x, y, 0)^\top\|_2$. Applying the range compression and the stationary phase approximation yields the range compressed data

$$d(t, s) = \tilde{d}(t, s) * p^*(-t) \approx T \text{rect}\left(\frac{s}{L}\right) \text{sinc}\left(\frac{2\pi B}{c} \left(t - \frac{2R(s, x_t, y_t)}{c}\right)\right) \cdot e^{-4\pi i f_c R(s, x_t, y_t)/c} \quad (2)$$

of one point target. Note that the antenna pattern is not considered in this signal model.

III. ROTATED OMEGA-K WITH EXPLICIT RANGE-MIGRATION CORRECTION

The rotated Omega-K algorithm with explicit range-migration correction [5] was developed to perform a second order motion compensation [6], see Figure 1. After the Stolt interpolation the SAR data $D = \mathcal{F}_{t,s}\{d\}$ in 2D frequency domain (k_r, k_x) is rotated by θ_s through

$$\begin{pmatrix} \tilde{k}_r \\ \tilde{k}_x \end{pmatrix} = \begin{pmatrix} \sin \theta_s & \cos \theta_s \\ \cos \theta_s & -\sin \theta_s \end{pmatrix} \begin{pmatrix} k_r \\ k_x \end{pmatrix}$$

to remove the effect of the squint angle. Subsequently a shift

$$\check{k}_r = \tilde{k}_r - \sqrt{k_c^2 - \tilde{k}_x^2}$$

with center wavenumber $k_c = 2f_c/c$ allows to separate the matched filter function H into two independent parts: H_{rmc} , which realizes the explicit range-migration correction and H_{az} :

$$H_{rmc}(\check{k}_r, \tilde{k}_x) = e^{-ir_0 \left(\sqrt{k_c^2 + (\check{k}_r + \sqrt{k_c^2 - \tilde{k}_x^2})^2} - \check{k}_r \right)},$$

$$H_{az}(\check{r}, \tilde{k}_x) = e^{i\check{r} \sqrt{k_c^2 - \tilde{k}_x^2}}.$$

Thus, the SAR image can be processed by

$$I(\check{r}, \tilde{x}) = \int_{\mathbb{R}^2} D(\check{k}_r, \tilde{k}_x) H_{rmc}(\check{k}_r, \tilde{k}_x) \cdot \mathcal{F}_{\check{r}}\{H_{az}(\check{r}, \tilde{k}_x)\} e^{i(\check{k}_r \check{r} + \tilde{k}_x \tilde{x})} d\check{k}_r d\tilde{k}_x, \quad (3)$$

$$\cdot \mathcal{F}_{\check{r}}\{H_{az}(\check{r}, \tilde{k}_x)\} e^{i(\check{k}_r \check{r} + \tilde{k}_x \tilde{x})} d\check{k}_r d\tilde{k}_x, \quad (4)$$

where r_0 is reference range to the scene center. Note that in equation (3) the factor resulting from the integral transformations is neglected, because it is approximately one [3].

The second order MoCom [6] operates on the range-migration corrected data, see Figure 1. It compensates the residual phase error remaining from the first order MoCom [4] by a modulation of

$$H_2(\check{r}, \tilde{x}) = e^{-4\pi i f_c / c (\phi_t(\check{r}, \tilde{x}) - \phi_c(\tilde{x}))}, \quad \text{with}$$

$$\phi_t(\check{r}, \tilde{x}) = \Delta y(\tilde{x}) \cos \theta_s \cos \theta_D(\check{r}) - \Delta h(\tilde{x}) \cos \theta_s \sin \theta_D(\check{r}),$$

$$\phi_c(\tilde{x}) = \Delta y(\tilde{x}) \cos \theta_s \cos \theta_D - \Delta h(\tilde{x}) \cos \theta_s \sin \theta_D,$$

which depends on the distance \check{r} to every range cell. Thus, not only the spot center but also approximately the whole scene is focused.

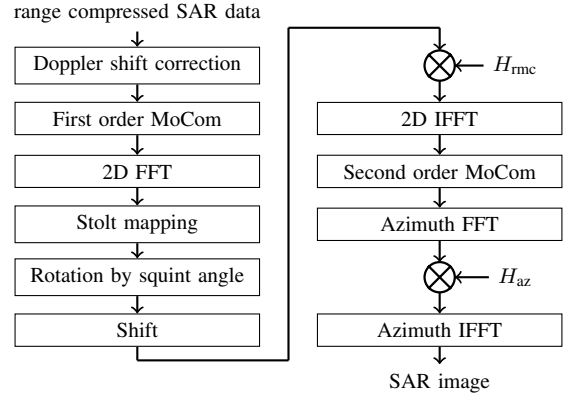


Fig. 1: Flowchart of rotated Omega-K with explicit range migration including first order and second order motion compensation.

IV. IMAGESHIFT IN FREQUENCY DOMAIN

Images, processed by Omega-K, are usually centered in the scene center \mathbf{p}_s and show the whole scene, see Figure 2. However, if only a small part of the scene has reflectors, like in our synthetic case, the center \mathbf{p}_c of this region containing them can be shifted to the image center by the well known Fourier transform shift theorem. The shifted image is calculated by

$$I(\check{r}, \tilde{x}) = \int_{\mathbb{R}^2} D(\check{k}_r, \tilde{k}_x) H_{rmc}(\check{k}_r, \tilde{k}_x) \mathcal{F}_{\check{r}}\{H_{az}(\check{r}, \tilde{k}_x)\} \cdot e^{i(\check{k}_r \check{r}_0 + \tilde{k}_x \tilde{x}_0)} e^{i(\check{k}_r \check{r} + \tilde{k}_x \tilde{x})} d\check{k}_r d\tilde{k}_x,$$

compare equation (3). The shift vector $(\check{r}_0, \tilde{x}_0)^\top$ lies in the evaluation plane and is calculated by

$$(\check{r}_0, \tilde{x}_0)^\top = m(\mathbf{p}_s) - m(\mathbf{p}_c).$$

By taking into account the individual depression angle $\theta_d(\mathbf{p}_c)$, $m : \mathbb{R}^3 \rightarrow \mathbb{R}^2$ maps points from the ground xy -plane to the evaluation $\check{r}\check{x}$ -plane by

$$m(\mathbf{p}_c) = E R_s R_d[\mathbf{p}_c] (\mathbf{p}_c - \mathbf{p}_f)$$

with

$$R_d[\mathbf{p}_c] = \begin{pmatrix} 1 & 0 & 0 \\ 0 & \sin \theta_d(\mathbf{p}_c) & \cos \theta_d(\mathbf{p}_c) \\ 0 & \cos \theta_d(\mathbf{p}_c) & -\sin \theta_d(\mathbf{p}_c) \end{pmatrix},$$

$$R_s = \begin{pmatrix} \sin \theta_s & \cos \theta_s & 0 \\ \cos \theta_s & -\sin \theta_s & 0 \\ 0 & 0 & 1 \end{pmatrix},$$

$$E = \begin{pmatrix} 1 & 0 & 0 \\ 0 & 1 & 0 \end{pmatrix}$$

and flight path center \mathbf{p}_f , which is its mid way point. Given that our only reflector is at \mathbf{p}_c , we can accelerate the SAR image computation by processing for example only $8k \times 8k$ relevant pixels instead of all $64k \times 8k$. In summary this translation enables us to process small parts of the scene with Omega-K to reduce computational time.

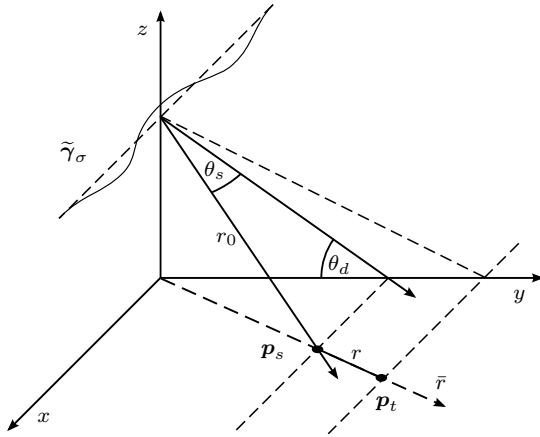


Fig. 2: Squinted spotlight SAR geometry. Relationship between perturbed flight path $\tilde{\gamma}_\sigma$, squint angle θ_s , depression angle θ_d , spot center \mathbf{p}_s , position \mathbf{p}_t of point target, ground range distance r along the \check{r} -direction and reference range r_0 .

V. GLOBAL BACKPROJECTION

The global Backprojection algorithm [12] operates in time domain (t, s) , which is why images with arbitrary size and image-resolution can be processed.

In a preprocessing step an image grid has to be defined. We rotate this grid in the xy -plane by the angle θ_g about the coordinates \mathbf{p}_c to reverse the effect of the squint angle θ_s . Subsequently a high-pass filtering of the range compressed baseband data d reverses the general smoothing effect of the integral operator inside the data acquisition process described by equation (1). A shift to the high frequency band of the filtered data yields the filtered range profile

$$q(t, s) = \mathcal{F}_t^{-1} \left\{ \pi |\omega| \mathcal{F}_t \{d(t, s)\} \right\} e^{2\pi i f_c t}. \quad (5)$$

A pulse by pulse mapping backwards to the predefined grid on the ground creates the image

$$I(x, y) = \int_{\mathcal{L}} q\left(\frac{c}{2} R(s, x, y), s\right) ds. \quad (6)$$

In this mapping the exact distance $R(s, x, y) = \|\tilde{\gamma}_\sigma(s) - (x, y, 0)^\top\|_2$ from platform position $\tilde{\gamma}_\sigma(s)$ to every pixel center in world coordinates $(x, y, 0)^\top$ is used. Hence, no additional motion compensation is necessary and no restriction on the scene size has to be considered. Our implementation of the global Backprojection algorithm is based on Gorham's implementation [12].

VI. NUMERICAL EXPERIMENTS

We compare the quality of SAR images processed by the rotated Omega-K algorithm with explicit range-migration correction and the global Backprojection algorithm.

For different magnitudes of motion errors, ground range distances to the spot center, squint angles and depression angles we generate synthetic, range compressed data by equation (2) and apply the rotated Omega-K algorithm with explicit range cell migration correction and the global Backprojection algorithm. The parameters of our simulated airborne X-band SAR system are listed in Table I.

TABLE I: Parameters of simulated X-band SAR system.

Parameter	Value
Carrier frequency f_c	9.6 GHz
Pulse bandwidth B	600 MHz
Pulse duration T	6 μ s
Sampling frequency f_s	600 MHz
Platform velocity v_0	100 m/s
Synthetic aperture length L	400 m
Pulse repetition frequency prf	2000 Hz
Flying duration T_f	4 s

Each squint angle $\theta_s \in \{0^\circ, 10^\circ, 20^\circ, 30^\circ\}$ and each depression angle $\theta_d \in \{15^\circ, 25^\circ, 35^\circ\}$ results in a scene with reference range $r_0 = 10\,000$ m. Furthermore, we describe the motion errors by the discretized standard deviation $\sigma = 0, 0.5, \dots, 5$ m of the perturbed flight path $\tilde{\gamma}_\sigma$. These motion errors have the highest impact regarding spatial resolution on points along the \check{r} -direction, see Figure 2. Thus, we choose the discretized ground range distance $r = 0, 50, \dots, 500$ m as the distance from the spot center \mathbf{p}_s to the position \mathbf{p}_t of the point target along \check{r} . Altogether, for every tuple $(\theta_s, \theta_d, r, \sigma)$ we compute the 1D azimuth ISLR

$$\text{ISLR} = 10 \log_{10} \left(\frac{P(-20 \delta_x, -\delta_x) + P(\delta_x, 20 \delta_x)}{P(-\delta_x, \delta_x)} \right)$$

with

$$P(a, b) = \int_a^b |I(\check{r}_0, \check{x})|^2 d\check{x},$$

where \check{r}_0 is the range cell with maximal energy and δ_x the spatial resolution in azimuth. No window function is used for side lobe suppression. Motion errors are generated by a random process, so we repeat this imaging process for every tuple $(\theta_s, \theta_d, r, \sigma)$ a few times and calculate the mean ISLR value.

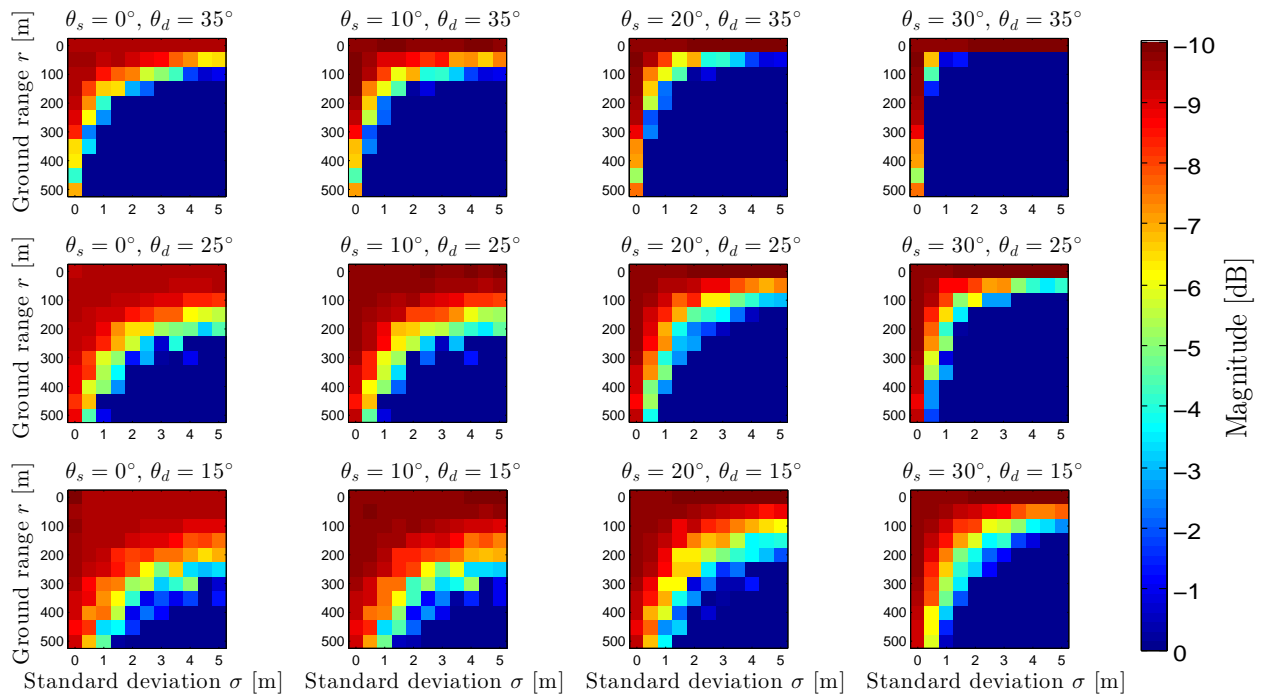


Fig. 3: Mean 1D azimuth ISLR of rotated Omega-K algorithm with explicit range cell migration correction. Every image visualizes the spatial resolution for a scene with fixed squint angle θ_s and fixed depression angle θ_d . To achieve a clear scaling we set positive ISLR values to zero. The standard deviation σ of motion errors is plotted along the x -axis and the ground range distance r to the spot center along the \bar{r} -direction is plotted along the y -axis, see Figure 2.

VII. RESULTS

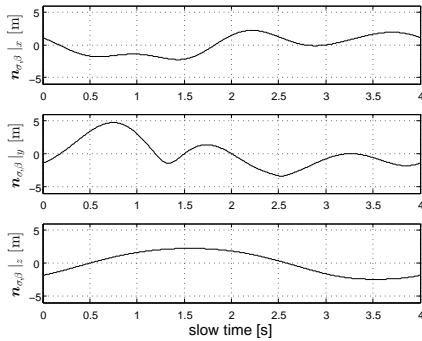
The results of our numerical experiments are given in Figure 3, where the sub-figure in the lower left corner presents the case with smallest squint angle $\theta_s = 0^\circ$ and smallest depression angle $\theta_d = 15^\circ$. In each direction, the squint angle θ_s and the depression angle θ_d increase up to $\theta_s = 30^\circ$ and $\theta_d = 35^\circ$ in the upper right sub-figure. The x -axis of every sub-figure describes the standard deviation σ of motion error, whereas the y -axis in every sub-figure shows the ground range distance r to the spot center. Altogether, Figure 3 shows the 1D azimuth ISLR depending on different squint angles, depression angles, standard deviation of motion errors and ground range distances to the spot center.

It can be seen in the lower left sub-figure that for $\theta_s = 0^\circ$ and $\theta_d = 15^\circ$ Omega-K yields good image quality even for $\sigma = 4$ m, which means approximately 8 m motion error magnitude, and a scene diameter greater than 300 m. By increasing only the squint angle θ_s to 30° the lower right sub-figure shows that Omega-K yields acceptable image quality with an ISLR < 3 dB for again $\sigma = 4$ m. However, this applies only up to 100 m scene diameter, which is clearly a smaller scene size than in the zero-squint case. Additionally, by increasing the depression angle θ_d the image quality decreases drastically for all θ_s . In the case of high depression angle $\theta_d = 35^\circ$ small flight path deviations cause large image errors. For a squint angle $\theta_s = 30^\circ$ and a depression angle $\theta_d = 35^\circ$ only a small area around the spot center is well focused for all motion error levels. This means that the value of the depression angle crucially impacts the image quality in the presence of motion errors for the Omega-K algorithm.

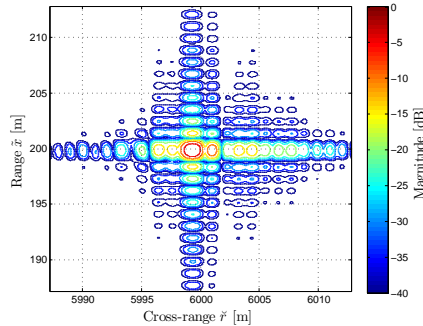
In general, this result verifies that the bigger the motion errors or the scene size, the lower the azimuth ISLR of the images generated with Omega-K. The specific behavior of the ISLR value as a function of motion errors and scene size mainly depends on the squint angle and the depression angle. By increasing the squint angle θ_s or depression angle θ_d the applicable range of motion error magnitude and scene size decrease for the Omega-K algorithm. In particular, if no motion errors occur, a scene with more than 500 m diameter can be processed with almost optimal spatial resolution. Additionally, for all motion error levels the spot center is focused. However, in presence of motion errors the spatial resolution decreases with increasing scene size depending on the motion error magnitude.

On the contrary the Backprojection algorithm preserves spatial resolution up to more than 500 m scene diameter and more than 10 m maximal motion error magnitude ($\sigma \approx 5$ m).

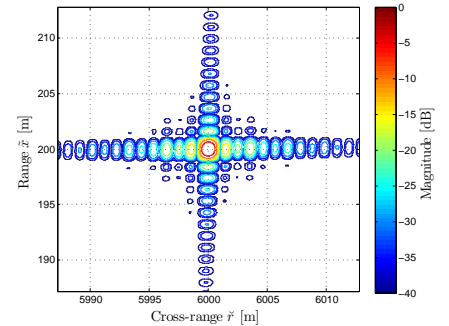
We illustrate our results on one example with parameters $\theta_s = 20^\circ$, $\theta_d = 25^\circ$, $r = 200$ m and $\sigma = 3$ m. Figure 4(a) shows the perturbed flight path. The corresponding SAR images processed with Omega-K and Backprojection are represented in Figure 4(b) and 4(c). The result in Figure 4(c) is always as good as the ideal case, whereas in Figure 4(b), effects of motion errors still can be seen.



(a) Generated motion errors for $\sigma = 3$ m in x, y, z dimension.



(b) Omega-K algorithm yields an ISLR = -3.58 dB.



(c) Backprojection algorithm yields an ISLR = -8.12 dB.

Fig. 4: Simulation results for one point target with ground range distance $r = 200$ m to spot center.

VIII. CONCLUSION

In summary, we have shown that depending on the squint and depression angles the quality of an image processed with Omega-K decreases with increasing magnitude of the motion errors and increasing ground range distance to the spot center. Based on these parameters and the required 1D azimuth ISLR we can predict the applicability of Omega-K. For example for a squint angle of 30° , a depression angle of 15° , motion errors with a magnitude greater than 5 m and targets located further away from the spot center than 300 m, Omega-K cannot guarantee acceptable spatial resolution for an X-band SAR system. In this case the Backprojection algorithm yields almost perfect image quality with the disadvantage of high computational cost.

REFERENCES

- [1] I. A. Cumming, F. H. Wong, *Digital Processing of Synthetic Aperture Radar Data - Algorithms and Implementation*, 1-th edition, Artech House, Boston, 2005.
- [2] D. C. Munson Jr., J. D. O'Brien, W. K. Jenkins, "A Tomographic Formulation of Spotlight-Mode Synthetic Aperture Radar", *Proceedings of the IEEE*, Vol. 71, No. 8, pp. 917–925, August 1983.
- [3] C. Cafforio, C. Prati, F. Rocca, "SAR data focusing using seismic migration techniques", *IEEE Transactions on Aerospace and Electronic Systems*, Vol. 27, No. 2, pp. 194–207, March 1991.
- [4] M. P. Nguyen, "Refined Motion Compensation for Highly Squinted Spotlight Synthetic Aperture Radar", pp. 738–741, 2012.
- [5] M. P. Nguyen, "Range Cell Migration Correction for Phase Compensation of Highly Squinted SAR", *VDE VERLAG GMBH, Berlin*, pp. 81–84, 2014.
- [6] M. P. Nguyen, *Bewegungskompensation und Autofokussierung von SAR-Rohdaten mit großem Schielwinkel*, VDI Verlag, Düsseldorf, 2014.
- [7] V. T. Vu, T. K. Sjögren, M. I. Pettersson, "A Comparison between Fast Factorized Backprojection and Frequency-Domain Algorithms in UWB Lowfrequency SAR", *Geoscience and Remote Sensing Symposium, IGARSS, IEEE International*, Vol. 4, pp. 1284-1287, 2008.
- [8] A. J. Hunter, M. Hayes, P. Gough, "A Comparison of Fast Factorised Back-Projection and Wavenumber Algorithms for SAS Image Reconstruction", *World congress on ultrasonics, Societe Francaise d'Acoustique*, pp. 527-530, 2003.
- [9] M. Cheney, B. Borden, *Fundamentals of Radar Imaging*, SIAM, Philadelphia, 2009.

- [10] P. Berens, *Neue Signalverarbeitungsverfahren für SAR im Scheinwerfermodus*, Shaker Verlag, 2003.
- [11] S. H. Park, J. I. Park, K. T. Kim "Motion Compensation for Squint Mode Spotlight SAR Imaging using Efficient 2D Interpolation", *Progress In Electromagn. Research*, Vol. 128, pp. 503–518, 2012.
- [12] L. A. Gorham, L. J. Moore, "SAR image formation toolbox for MATLAB", *Proc. SPIE, Vol. 7699, Algorithms for Synthetic Aperture Radar Imagery XVII*, 2010.